J Mater Sci (2007) 42:2455–2462
DOI 10.1007/s10853-006-1239-5

Multi-technique and multi-scale approach applied to study the structural behavior of heterogeneous materials: natural SiO_2 case

L. Khouchaf · J. Verstraete

Received: 21 September 2005 / Accepted: 6 February 2006 / Published online: 23 December 2006

Abstract A multi-technique and multi-scale approach have been initiated to study the structural properties of a natural heterogeneous material. This approach has led us to introduce the concepts of long-range order LRO and short-range order SRO. The correlation between these concepts has enabled us to advance in the comprehension of the mechanisms of degradation of natural SiO_2 aggregate submitted to the process of the alkali–silica reaction (ASR). On LRO scale, the structural changes of the aggregate are revealed by the reduction of the size of grains, which means that the attack starts by affecting amorphous and poorly crystallized zones. This phenomenon generates the formation of very unstable amorphous and nanocrystallized products, which take part in the degradation of the aggregate. On SRO scale tetrahedral environment of silicon atoms is preserved in spite of the introduction of OH^- ions with a relaxation phenomenon. The second layer of coordination around silicon remains almost unchanged. These results add new information showing that ASR must be considered as a multi-scale process. The methodology itself may be extended to other problems.

Introduction

The durability of a material is closely related to its structural properties [1]. The study of these properties is of great importance in the field of materials science. These properties can be classified according to various scales such as: macroscopic, microscopic, nanometric and atomic. The classification according to various scales of these properties shows the need to use several techniques able to probe each of these scales. It is more difficult when the material to study is heterogeneous. Accordingly, we initiated a multi-technique and multi-scale approach in order to study structural properties of a natural heterogeneous material such as SiO_2 flint. SiO_2 compounds are used for several applications. In particular, SiO_2 is a major component of concrete. One phenomenon, which takes part in the degradation of the concrete is called alkali–silica reaction (ASR) [2–8]. Several works have been carried out in order to study the effects of the ASR process in the degradation of concrete containing SiO_2 as an aggregate type [2–8]. The structural behavior of SiO_2 aggregate during its degradation is a good parameter in the evaluation of the durability of the concrete [9]. The formation and the evolution of amorphous and poorly crystallized phases could induce a variation of the volume of the aggregate and consequently participate in its swelling, which could cause the rise of internal stresses in the concrete [8]. In the same way, a correlation between the expansion of the concrete, the particle size and the surface area of the aggregate has been shown [10].

Alkali–silica reaction can be described as a physicochemical process between various components of concrete such as the siliceous phases containing SiO_2, some alkaline K^+ and/or Na^+ and Ca^{2+} cations. The explanation of the mechanism(s) of the degradation of concrete by ASR process is not cleared up [6–8]. Indeed, the effects of ASR can be expressed on a

L. Khouchaf (✉) · J. Verstraete
Centre de Recherche de l'Ecole des Mines de Douai,
941, rue Charles Bourseul, BP.838, 59508 Douai, France
e-mail: khouchaf@ensm-douai.fr

macroscopic scale (crack,..), on a microscopic one (modification of the size and the microstructure of the grains) and nanometric one (structural and chemical changes of the resulting phases). Thus, ASR must be considered as a multi-scale process. Long-range order (LRO) and short-range order (SRO) concepts coupled, are a good way to study the structural properties of materials either in crysallized and/or in amorphous state. When LRO concept needs different techniques such as X-ray diffraction (XRD) and Scanning Electron Microscope (SEM) for example, SRO concept needs techniques such as Extended X-ray Absorption Fine Structure (EXAFS), X-ray Absorption Near Edge Structure (XANES) and Nuclear Magnetic Resonance (NMR). Ersen et al. [11] showed the interest of LRO and SRO concepts to study the structural behavior of iron and cobalt disilicides thin films. Christie et al also introduced another concept called MRO ''medium-range order'' concept to investigate structural characteristics of positionally disordered lattices applied to the first sharp diffraction peak in glasses [12]. They contributed to explain the origin of the vitreous halo, which appears in the XRD patterns of the amorphous SiO_2.

In this paper our approach will be applied to study the structural behavior of SiO_2 aggregate induced by ASR process as taking part in concrete degradation. Techniques such as Environmental SEM, XRD, XANES, EXAFS and NMR will be performed to do so.

Experimental

Environmental Scanning Electron Microscope (ESEM)

Because our aggregate is insulating, Environmental SEM was used to carry out images [13–15]. ESEM used is an ''ElectroScan 2020'' type equipped with an Energy Dispersive Spectrometer EDS Microanalysis system ''Oxford Linkisis''. The electron source is a tungsten filament. The accelerating voltage is fixed at 20 kV with an emission current of 49 μA. A long ESD detector at a 19 mm working distance is used in order to reduce the skirt beam phenomena. The chamber pressure is varied by introducing water-vapour gas.

X-ray diffraction

XRD spectra were recorded for 2θ values between 10° and 100° with a step size of 0.007° and a counting time of 10 s per step using a Bruker D8 Advance diffractometer operating at 40 kV and 40 mA with Co radiation ($\lambda \approx 1.78897$ Å) [7].

X-ray absorption: XANES, EXAFS

XANES and EXAFS measurements have been performed at the SA32 beam-line of the Super-ACO ring at LURE, Orsay, France. Synchrotron radiation was monochromatized by a double-crystal monochromator, equipped with two InSb (111) single crystals, and calibrated on a c-Si sample (1,839 eV at the Si K-edge threshold). The spectra were obtained in the total electron yield (TEY) detection mode, and were taken with a 0.2 eV step for XANES and 1 eV step for EXAFS at high vacuum 10^{-6} mbar [16–20].

Nuclear magnetic resonance

^{29}Si MAS-NMR spectra were obtained using a Bruker MSL 300 spectrometer operating at 59.631 MHz with a 2.5 mm Bruker CP/MAS probe spinning at 4 kHz. Tetramethylsilane (TMS) was used as a reference for chemical shifts measurements. Spectra were recorded with a pulse angle of 30° and a recycle delay of 80 s. The number of scans was 2,150 for each sample [9].

Material

The aggregate studied is a natural flint with 99.1% of SiO_2 revealed by X-ray fluorescence analysis and has a disordered crystallographic structure compared to alpha quartz. The aggregate has been submitted to a procedure attack by ASR process which have been previously described [7] but are briefly summarized here. The aggregate (1 g of crushed flint) was subjected to accelerated ASR at 80 °C with a mixture of 0.5 g of portlandite $Ca(OH)_2$ and 10 ml of potash solution KOH at 0.79 mol/l.

In the ASR mechanism, the hydroxyl, potassium and calcium ions contained in the solution within the concrete pores, poorly penetrate crystallized parts of the aggregate [21]. The attack is initiated by hydroxyl ions and usually schematized by the equation below:

$$2SiO_2 + OH^- \rightarrow SiO_{5/2}^- + SiO_{5/2}H \quad (1)$$

inducing the rupture of Si–O–Si bonds between two tetrahedra called Q_4 and producing negatively charged $SiO_{5/2}^-$ species and $SiO_{5/2}H$ species called silanols (Fig. 1). The cations, which are abundant in the pores,

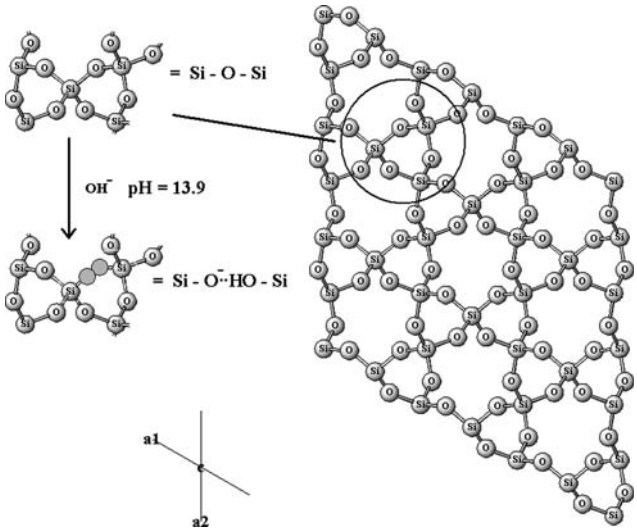

Fig. 1 Schematic diagram showing the rupture of the Si–O–Si bonds in SiO_2 compound

are attracted to the sites of negative charge and participate in the reaction.

Results

Long-range order study

In Fig. 2a and b ESEM's images represent some area of the SiO_2 aggregate before ASR attack. The presence of well-defined geometrical grains and other characterization using monocrystal XRD (not reported here) show that the aggregate is a polycrystalline material. Some defects can be observed (circled in Fig. 2b) which are characteristic of a porous and poorly crystallized material.

Figure 3 shows XRD patterns of the aggregate and C–SiO_2 used as a reference. For the aggregate, the pattern reveals that all the peaks of α-quartz are present with a decrease in intensity.

After ASR process the morphology of the aggregate has changed (Fig. 4). Some zones have been dissolved and others have different forms. The attacked aggregate is parceled out with a decrease of the grain size during ASR process. Some grains with a diameter of about 10 μm and under can be observed with higher magnification. They are hexagonal and can be attributed to SiO_2 grains with a good degree of cristallinity (zone Zc in Fig. 4). Other zones show not well-defined grains (zone Za in Fig. 4).

The defects observed in the attacked aggregate with ESEM's micrographs may be related to the changes of the crystallographic structure. During ASR process, the XRD patterns (Fig. 5) indicate a decrease in the intensities of the peaks and the presence of a vitreous halo located between 20° and 37° in 2θ.

The amorphous and nanocrystallized phases in the aggregate are a good finger-print showing that the reactivity of our aggregate is very much linked to its structural behavior.

Short range-order study

Why is it significant to perform a short range-order study? One point that most authors agree with is the fact that the starting process of the attack of the aggregate by ASR may follow Eq. 1. This equation shows that the structural environment of silicon atoms will be affected. But how? Currently this question remains unanswered. For this reason it seems necessary to study the short range-order around silicon atoms. Figure 6a and b represent the XANES spectra of the

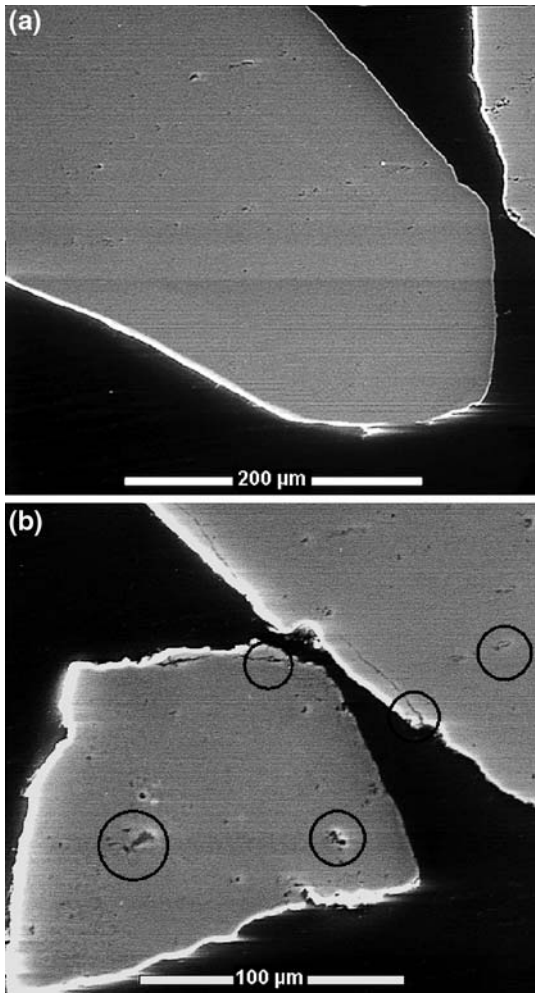

Fig. 2 ESEM micrographs of flint aggregate before ASR attack: (**a**) hexagonal form, (**b**) presence of defects

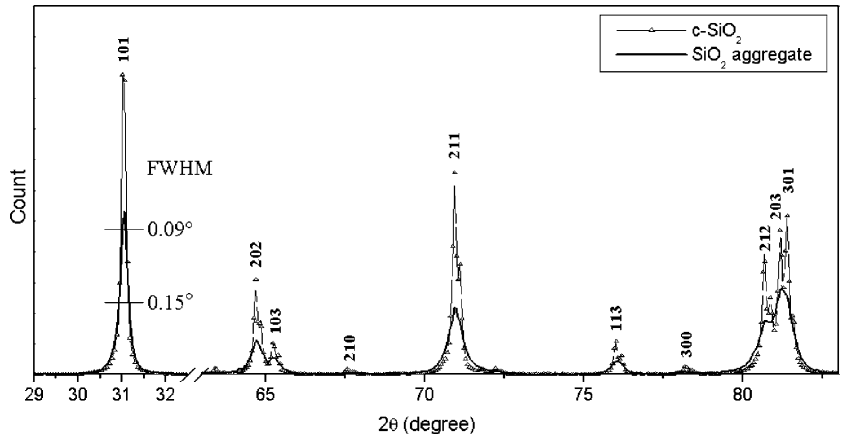

Fig. 3 X-ray diffraction patterns of C–SiO2 used as a reference and the flint aggregate before ASR attack

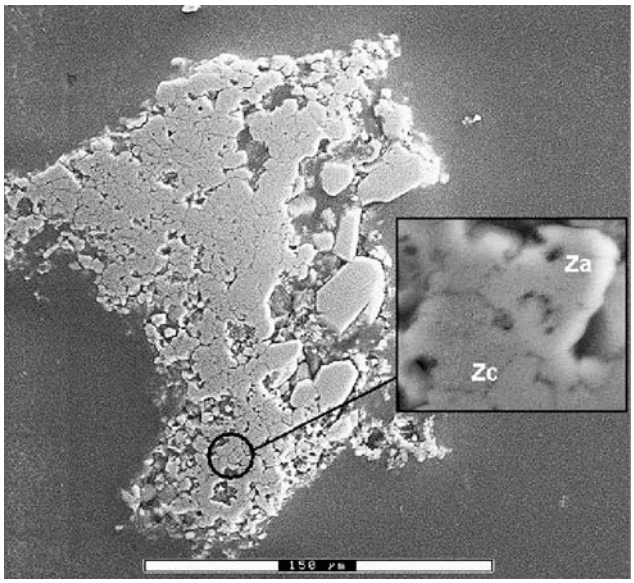

Fig. 4 ESEM micrograph of the aggregate after attack with Zc and Za zones

SiO_2 aggregate compared to those of C–SiO_2 and the XANES spectra of attacked SiO_2 aggregate compared to the one of the starting aggregate respectively.

XANES spectra of the samples show fine structure peaks such as A, B and C that are characteristic of the XANES spectrum of C–SiO_2 [17, 18]. The positions of the peaks A and B remain unchanged in the two spectra (Fig. 6a). Furthermore, the decrease of the magnitude of the fine structure peaks located between 1,850 and 1,860 eV is observed.

After aggregate attack by ASR the energy positions of peaks A and B remain unchanged (Fig. 6b). In addition, a substancial decrease of the amplitude in the aggregate of the peaks located between 1,850 and 1,860 eV after reaction is observed. But the disorder detected on a SRO scale in the starting aggregate is interesting and makes an attack of Si–O–Si bonds possible which may be considered as a factor explaining the origin of the aggregate reactivity.

In order to obtain radial distributions of different neighbors around silicon atoms, EXAFS experiments have been performed. The "*EXAFS pour le Mac*" software [22] was used to perform the initial data treatment. A sixth degree polynomial function was used to reproduce the atomic absorption, and the signal was normalized using the Lengeler–Eisenberger method. A k^2 weighting and a Kaiser apodization

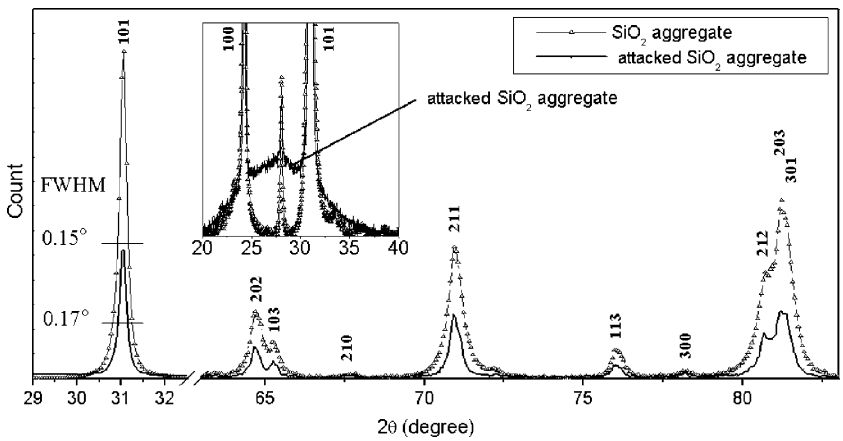

Fig. 5 X-ray diffraction patterns of the aggregate before and after reaction

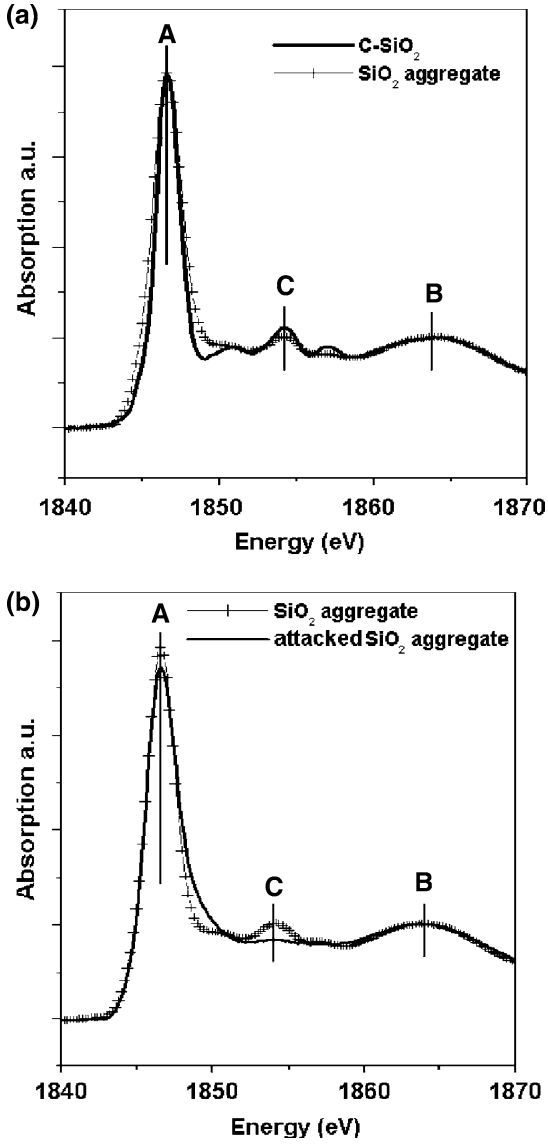

Fig. 6 Si–K XANES spectra of (**a**) C–SiO_2 used as a reference and the aggregate before attack, (**b**) the aggregate before attack and after attack

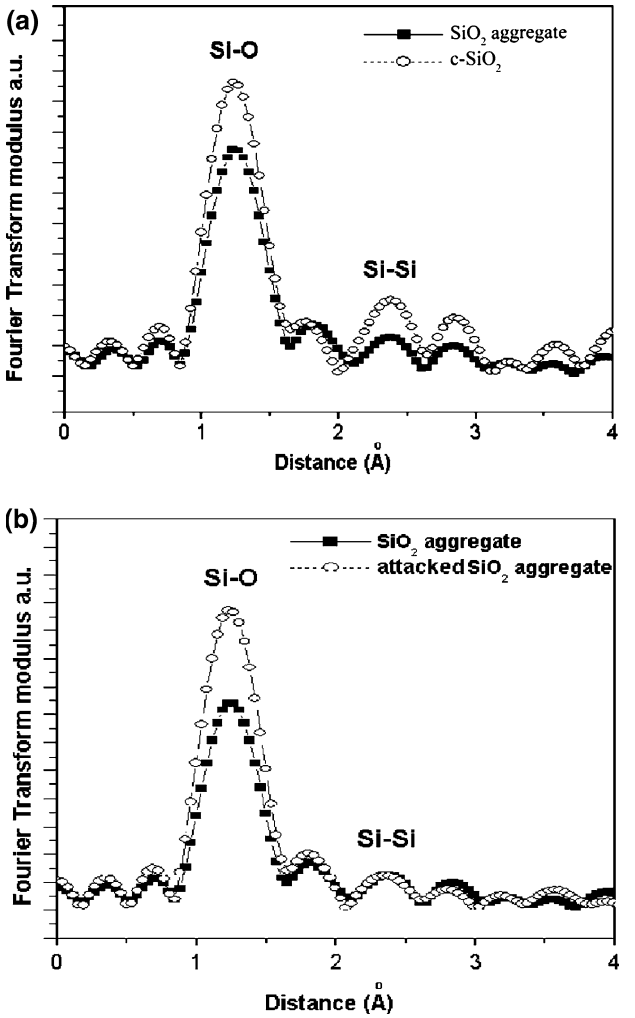

Fig. 7 EXAFS Fourier transforms modulus at Si–K edge from (**a**) C–SiO_2 used as a reference and the aggregate before attack, (**b**) the aggregate before attack and after attacks

window between approximately 2.8 and 11.3 $Å^{-1}$, with $\tau = 1.0$, were used to calculate the Fourier transform of the EXAFS signal shown here (Fig. 7a, b). C–SiO_2 was used as a reference. In C–SiO_2 each silicon atom is tetrahedraly coordinated by oxygen. SiO_4 tetrahedra show that the Si–O interatomic distances are distributed in two sites [23]. The presence of two values for Si–O distances shows that the tetrahedra in C–SiO_2 are asymmetric. As second neighbors each silicon atom is surrounded by four silicon atoms.

The EXAFS study enabled us to follow the evolution of SRO around silicon on a lower scale than the one obtained by XANES. Figure 7a and b show Fourier transforms of EXAFS signals (FT) of the SiO_2 aggregate compared to C–SiO_2 one and FT of attacked SiO_2 aggregate compared to starting aggregate one respectively. The amplitude of the first shell (Si–O) peak of starting aggregate is lower than the one of C–SiO_2 whereas the amplitude of the attacked aggregate increases. Moreover the amplitude of the second peak and Si–Si distance in attacked aggregate (Fig. 7b) remain almost unchanged in spite of the process of breaking up of Si–O–Si bonds announced by Eq. 1.

In order to improve our understanding on a SRO scale, the chemical environment of silicon has been investigated by ^{29}Si NMR MAS. Indeed, NMR is a very useful tool to distinguish between Si–O and Si–OH bonds. Figure 8 shows NMR spectra of the starting aggregate and the attacked aggregate.

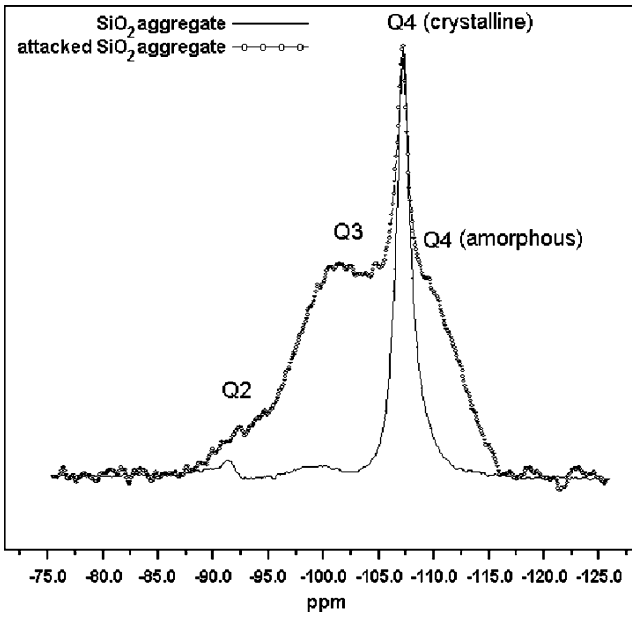

Fig. 8 MAS NMR ^{29}Si spectra of the aggregate before attack and after attack

NMR analysis of the starting aggregate shows the presence of three tetrahedral environments. The main peak at 107 ppm is related to Q_4 (crystalline) sites [24, 25]. The other peaks are related to Q_3 (silanols) and Q_2 sites. During the ASR process the increase in the intensity of the peak of Q3 sites is observed while another peak of Q4 (amorphous) sites at 110 ppm is rising.

Discussion

On LRO scale, the presence of well-defined geometrical grains shown by ESEM's micrographs and other characterization using monocrystal XRD indicate that the aggregate is a polycrystalline material. Some defects can be observed (circle in Fig. 2b) which are characteristic of a porous and poorly crystallized material. A previous study showed that the structural properties of alpha quartz C–SiO_2 are not sensitive to the external attack whereas Mehta and Monteiro [26] have reported that natural aggregates such as the flint could be attacked by ASR process.

Thus, the defects present within the aggregate will play a substantial role during ASR attack. Currently, the connection between the structural properties of such compounds and their degree of reactivity have not been clearly assessed. In our approach XRD analysis coupled with ESEM observations is able to improve our knowledge on a LRO scale about some causes and effects concerning the reactivity of the aggregate. As it has been reported by the studies undertaken by Poole [5] and Liang [27], we can indicate that a close connection must exist between the crystallinity of our aggregate and its degree of reactivity.

After ASR process the morphology of the aggregate has changed (Fig. 4). Some zones have been dissolved and others have different forms. The attacked aggregate is parceled out with a decrease of the grain size during ASR process. Some grains with a diameter of about 10 μm and under can be observed with higher magnification. They are hexagonal and can be attributed to SiO_2 grains with a good degree of crystallinity (zone Zc in Fig. 4). Other zones do not show well-defined grains (zone Za in Fig. 4). The presence of the vitreous halo is attributed to the presence of the amorphous and nanocrystallized phases in our material [12, 28]. The irregular shapes present in Fig. 4 (zone Za) could be correlated to the presence of the vitreous halo. In a previous study [8], a decrease of the full width at half-maximum (FWHM) has also been observed during the reaction. This reduction has been attributed to the appearance of zones in which the degree of crystallinity is improving (zone Zc in Fig. 4).

The defects observed in the starting aggregate with ESEM's micrographs and the rise of the vitreous halo after attack which is attributed to the presence of the amorphous and nanocrystallized phases in our aggregate are a good finger-print showing that the reactivity of our aggregate is very much linked to its structural behavior. Such results show that ASR may be considered as a process generating amorphous and nanocrystallized phases.

On SRO scale, the energy positions of the peaks A and B in the XANES spectra of the aggregate are the same compared to the one in C–SiO_2 which indicate that silicon atoms are in a tetrahedral environment (Fig. 6a). Furthermore, the decrease of the magnitude of the fine structure peaks located between 1,850 and 1,860 eV is able to reveal an amorphous behavior around silicon atoms on a SRO scale. As a result the widening of peak A may be attributed to an important disorder in the starting aggregate on a SRO scale.

After aggregate attack by ASR the energy positions of the peaks A and B in the XANES spectra of the aggregate remain unchanged (Fig. 6b) showing that the tetrahedral environment is preserved. This result is important because it was supposed in a previous study [29] that the breaking up of the Si–O–Si bonds should be accompanied by an increase in the coordination number of the silicon atoms resulting from the introduction of OH^- ions in their vicinity. XANES spectra do not show any changes in coordination number. But the disorder detected on a SRO scale in the starting

aggregate is interesting and makes an attack of Si–O–Si bonds possible which may be considered as a factor explaining the origin of the aggregate reactivity. Besides the increase in disorder in the attacked SiO_2 aggregate agrees with the rise of an amorphous phase observed by XRD and ESEM on a LRO scale.

As indicated above, let's consider C–SiO_2 structure; each silicon atom is tetrahedraly coordinated by oxygen. SiO_4 tetrahedra show that the Si–O interatomic distances are distributed in two sites [23]. The presence of two values for Si–O distances shows that the tetrahedra in C–SiO_2 are asymmetric. As second neighbors each silicon atom is surrounded by four silicon atoms. In the case of the starting aggregate, the low amplitude of FT compared to that of C–SiO_2 reveals a disorder, which is in agreement with XANES results. It is important to point out that our approach enables us to show the multi-scale disorder that exists in the aggregate structure and that may explain its reactivity. As FT amplitude of the first distribution due to oxygen contribution increases after ASR process (Fig. 7b), we know thanks to the XANES result, that silicon atoms remain tetrahedrally coordinated by oxygen. Furthermore, the increase of the FT amplitude of the first distribution in attacked aggregate cannot be due to an increase of its coordination number in the first shell. Moreover the amplitude of the second peak and Si–Si distance in attacked aggregate (Fig. 7b) remain almost unchanged in spite of the process of breaking up of Si–O–Si bonds announced by Eq. 1. The absence of modification in the Si–Si distances as shown by EXAFS analysis cannot confirm that the starting process of the ASR must be described by Eq. 1 only. It appears that Eq. 1 is not sufficient to describe the mechanism of structural changes induced by ASR process.

On a SRO scale, these results, together with the decrease in the intensity of the peak C in XANES spectra (Fig. 6b), agree with those obtained on a LRO scale such as the rise of a vitreous halo in the XRD pattern and the presence of zones with not well-defined forms in the attacked aggregate (zone Za in Fig. 4). NMR analysis and XRD patterns show that the attacked aggregate is composed of an amorphous phase which is a mixture of amorphous silica and silanols. From the point of view of EXAFS analysis, the increase in the amplitude of the FT related to the first shell may be attributed to an increase of the order within the first shell which may be explained by the presence of the Q3 and the Q4 (amorphous) as indicated by NMR results. In fact, it is well known that the order within the SiO_4 tetrahedra of an amorphous silica is better than at of a C–SiO_2. Indeed, as indicated above, in C–SiO_2 and in aggregate before attack, the SiO_4 tetrahedron is asymmetric (there are two Si–O distances). This asymmetry introduces a reduction of the FT amplitude. After the attack of the aggregate, the amorphous fraction increases inducing the presence of one Si–O distance, which improves the symmetry of SiO_4 tetrahedra and introduces an increase in the FT amplitude of oxygen contribution (Fig. 7b). On the atomic scale, ASR process appears as a relaxation process that occurs on the Si–O bonds. This result is a demonstration in agreement with previous studies showing that the reactivity of amorphous silica is higher compared to the one of a crystalline material.

Conclusions

We initiated a multi-technique and multi-scale approach to study the structural properties of a natural and heterogeneous material. This approach has led us to introduce the concepts of LRO and SRO to follow structural evolution of SiO_2 aggregate submitted to ASR process. It has enabled us to advance in the comprehension of the mechanisms of deterioration of the SiO_2 aggregate under ASR process. The structural evolution of the aggregate is revealed on a LRO scale by the reduction of the size of grains, which started on the poorly crystallized grains. This phenomenon generates the formation of very unstable amorphous products, which take part in the degradation of the aggregate. On a SRO scale, the order in the first shell is improved and seems to be similar to the one in an amorphous aggregate. This result is important to explain the origin of the reactivity of an aggregate on a SRO scale. The second shell of atoms around silicon remains almost unchanged. The results obtained do not agree with the unique mechanism schematized by equation 1 to explain the structural changes of the SiO_2 aggregate submitted to ASR process. That is the reason why we have undertaken accurate studies taking into account the heterogeneous aspect of the aggregate and carrying out multi-scale investigations with multi-technique using micro-beam sources.

Acknowledgements Authors would like to thank Dr A.M. Flank and P. Lagarde for their help in performing XAS experience.

References

1. De Almaida P, Van Deelen J, Catry C, Sneyers H, Pataki T, Andriessen R, Van Roost C, Kroon JM (2004) Appl Phys A 79:1819
2. Chatterji S, Jensen AD, Thaulow N, Christensen P (1986) Cement Concrete Res 16:246

3. Wang H, Gillot JE (1991) Cement Concrete Res 21:647
4. Brouxel M (1993) Cement Concrete Res 23:309
5. Poole AB (1992) In: Proceedings of the 9th international conference on alkali-aggregate reaction, London (England). Concrete Society Publications Cs 104 1, p 782
6. Chatterji S, Thaulow N (2000) In: Berube MA et al (ed) Proceedings of the 11th international conference on alkali-aggregate reaction in concrete, Quebec (Canada), p 21
7. Verstraete J, Khouchaf L, Bulteel D, Garcia E-D, Flank AM, Tuilier MH (2004) Cement Concrete Res 34:581
8. Verstraete J, Khouchaf L, Tuilier MH (2004) J Mater Sci 39:20–6221
9. Khouchaf L, Verstraete J, Prado RJ, Tuilier MH (2005) Phys Scripta T115:552
10. Grattan PE-Bellew, Beaudoin JJ, Vallée VG (1998) Cement Concrete Res 28:8
11. Ersen O, Pierron-Bohnes V, Tuilier MH, Pirri C, Khouchaf L, Gailhanou M (2003) Phys Rev B 67:094116
12. Elliott SR (1991) Nature 354:445
13. Danilatos GD (1988) In: Fundations of environmental microscopy advances in electronics and electron physics, vol 71. Academic, New York, p 109
14. Khouchaf L, Verstraete J (2002) J Phys Iv 12:341
15. Khouchaf L, Verstraete J (2004) J Phys Iv 118:237
16. Lagarde P, Flank AM (1993) J-P Itié J Appl Phys 32:613
17. Li D, Bancroft GM, Kasrai M, Fleet ME, Feng XH, Tan KH, Yang BX (1993) Solid State Commun 87(7):613
18. Li D, Bancroft GM, Kasrai M, Fleet ME, Secco RA, Feng XH, Tan KH, Yang BX (1994) Am Mineral 79:622
19. Khouchaf L, Tuilier MH, Guth JL, Elouadi B (1996) J Phys Chem Solids 57:251
20. Levelut C, Cabaret D, Benoit M, Jund P, Flank A-M (2001) J Non-Crystalline Solids 293–295:100
21. Kurtis KE, Monteiro PJM, Brown JT, Meyer-Ilse W (1998) Cement Concrete Res 28(3):411
22. Michalovicz A (1991) In Logiciels Pour La Chimie. Société Française De Chimie, Paris, p102
23. Devine RAB, Duraud JP, Dooryhee E (2000) In: Structure and imperfection in amorphous and crystalline silicon dioxide. Wiley, New York, p 396
24. Xie XQ, Ranade SV, Dibenedetto AT (1999) Polymer 40:6297
25. Gendron-Badou A, Coradin T, Maquet J, Frohlich F, Livage J (2003) J Non-Crystalline Solids 316:331
26. Mehta PK, Monteiro PJM (1993) In concrete: structure, properties, and materials. Prentice Hall, Englewood Cliffs
27. Liang T, Meihua W, Sufen H, Mingshu H (1997) Adv Cement Res 9(34):55
28. Klug HP, Alexander LE (1959) In: X-ray diffraction procedures for polycrystalline and amorphous materials, second printing. Wiley, New York, p 586
29. Iler RK (1979) The chemistry of silica: solubility polymerization, colloid and surface properties and biochemistry of silica. Wiley, New York